

Femtocell Base Station Deployment in Commercial Buildings: A Global Optimization Approach

Jia Liu, *Member, IEEE*, Tianyou Kou, Qian Chen, and Hanif D. Serali

Abstract—While the deployment of femtocell in residential buildings has firmly positioned it as a major performance leap in wireless communications, its deployment in commercial buildings remains under-explored. In commercial building environments, the femtocell base station (FBS) placement planning is particularly challenging due to the impact of the building size, layout, structure, and wall/floor separation. In this paper, we study the problem of jointly optimizing FBS placement and power control in commercial building environments to prolong the battery life for mobile handsets. We first propose a mathematical model that captures the unique building features. Based on this model, we employ a set of novel transformation strategies to formulate the FBS placement problem as a mixed-integer convex program (MICP). Accordingly, we propose an effective global optimization algorithm based on using the convex relaxation of the formulated MICP within a branch-and-bound framework. This approach guarantees finding a global optimal solution. To demonstrate the efficacy of our algorithm, we conduct extensive numerical studies. Our proposed model and optimization approach offer useful insights into femtocell deployments in commercial buildings.

Index Terms—Femtocell networks, commercial buildings, base station placement, power control, battery life, nonconvex integer optimization, global optimization algorithms.

I. INTRODUCTION

Femtocells are low-cost, small-sized base stations (BS) that offer high quality voice/data services to indoor mobile handset users. Femtocell systems use the prevalent broadband Internet connections (e.g., DSL, cable, etc.) as a backhaul to connect users to the operator's core network or the Internet. As a result, not only do users enjoy better coverage due to the close vicinity to BSs, the network operators also benefit from a reduced demand for constructing macrocell towers. Due to this "win-win" situation, recent years have witnessed an increasing acceptance of femtocell systems. Currently, several standard bodies, such as 3GPP, 3GPP2, and WiMAX Forum (IEEE 802.16), have respectively started to standardize WCDMA, LTE, and WiMAX femtocells [1], [2]. Meanwhile, more than

10 major operators worldwide have commercially launched residential femtocell deployments [3].

While the first phase of residential deployment has firmly positioned femtocells as a major performance leap in wireless communications, it is envisioned that the next big wave of femtocell deployment will occur in commercial buildings, such as large enterprises, big-box stores, dormitories, malls, airports, and other public places [3]. The special features of commercial building environments bring many new challenges to femtocell deployments. Although research activities on femtocell systems have soared in recent years and many important results have been obtained (e.g., local area coverage [4], [5], synchronization and interference management [6], [7], [8], self-organization/configuration [9], [10], access and quality-of-service (QoS) control [11], [12], just to name a few), results targeted at femtocell networks in commercial buildings remain limited. In particular, *femtocell placement optimization in commercial buildings* is still under-explored.

Femtocell placement optimization in commercial buildings is important due to the high impact of the locations of femtocell base stations (FBS) on the *energy expenditure* of each mobile handset (HS). It is well-known that the transmission power of an HS depends heavily on the physical distance between the HS and its targeted base station. The poor battery life performance of current smartphone devices (less than eight hours even under moderate use [13], [14]) further indicates a compelling need to study femtocell placement optimization. However, unlike simple residential buildings, commercial buildings range from small offices to large-sized shopping malls with different building layouts and various wall and floor separations (e.g., open atriums, contained offices, hallways, or basements), which yield different signal path losses and multipath fading patterns and could require multiple FBSs. Also, special building safety codes and functional constraints could impose further restrictions to the FBS installation locations. Therefore, FBS placement planning is not only desirable, but also necessary to achieve satisfactory network performance. Due to the lack of results in this area, the main objective of this work is to obtain some fundamental understanding of the FBS placement problem in commercial buildings.

In this paper, we focus on the joint optimization of FBS placement to minimize the *uplink transmission power* of each HS, while ensuring network coverage and meeting each HS's QoS requirement. The main contributions of this work are as follows:

- We propose a mathematical model for joint FBS placement and uplink power control optimization in commercial buildings. Our model captures the unique floor attenuation factor (FAF) and FBS installation restrictions,

Manuscript received March 1, 2011; revised September 1, 2011; and accepted October 12, 2011. This work has been partially funded by NSF Grant CMMI-0969196.

Jia Liu and Tianyou Kou are with the Department of Electrical and Computer Engineering, The Ohio State University, Columbus, OH, 43210 USA (e-mail: liu@ece.osu.edu, kou.20@osu.edu). This work was conducted while Tianyou Kou was a graduate research assistant with the Construction Systems Management Program in the Department of Food, Agriculture, and Biological Engineering at The Ohio State University.

Qian Chen is with the Construction Systems Management Program in the Department of Food, Agriculture, and Biological Engineering, The Ohio State University, Columbus, OH, 43210 USA (e-mail: chen.1399@osu.edu).

Hanif D. Serali is with the Grado Department of Industrial and Systems Engineering, Virginia Tech, Blacksburg, VA, 24061 USA (e-mail: hanifs@vt.edu).

Digital Object Identifier xx.xxxx/JSAC.2012.xxxxx.

and provides a foundation for the study of the problem.

- Based on the proposed model, we show that the joint FBS placement and power control optimization problem can be formulated as a *mixed-integer nonconvex programming* problem (MINLP). Due to this integrality and nonconvexity, no existing optimization methods can be readily applied. To address this difficulty, we propose a set of novel reformulation strategies to transform the original MINLP problem into an equivalent *mixed-integer convex programming* (MICP) problem. This facilitates the design of effective optimization algorithms.
- For the equivalent MICP problem, we propose a global optimization approach based on its convex programming relaxation (CPR) and the branch-and-bound (BB) framework, which guarantees finding a global optimal solution. To demonstrate the efficacy of our algorithmic procedures, we conduct extensive computational studies. Our numerical results corroborate our theoretical analysis. The optimal solutions obtained by our proposed approaches offer useful insights into femtocell deployment in commercial buildings.

The remainder of this paper is organized as follows. We introduce our network model and problem formulation in Section II. Our global optimization approach is presented in Section III, including problem reformulation techniques, the BB/CPR algorithmic framework, and a symmetry-defeating strategy to enhance the convergence performance of BB/CPR. In Section IV, we present numerical results and Section V concludes this paper.

II. NETWORK MODEL AND PROBLEM FORMULATION

In this section, we first introduce the femtocell network model for commercial buildings in Section II-A. Then, in Section II-B, we establish a wireless signal path loss model that captures the unique features in commercial buildings. Based on this path loss model, we define constraints for network coverage and femtocell base station associations in Sections II-C and II-D, respectively. Finally, based on these mathematical models, we present the problem formulation in Section II-E.

A. Network Model

We consider a femtocell network in a commercial building consisting of M FBSs and N service areas (SA). Here, an SA could be any subregion in the building where users with mobile HS are able to sit (e.g., offices) or roam freely (e.g., hallways, atriums, etc), as illustrated in Fig. 1. For now, we assume that M is large enough to ensure network coverage. We will discuss how to determine an appropriate value of M in greater detail later in Section III-B. We denote the FBSs and SAs as FBS1, ..., FBS M and SA1, ..., SA N , respectively.

We now derive the distance relationship between an FBS and an SA, which is more complex than the conventional Euclidean distance due to the special features in buildings. First, since commercial buildings are likely to have multiple floors, the coordinates of FBSs and HSs are in 3-D space. We use (u_i, v_i, w_i) , $i = 1, \dots, N$, to denote the coordinates of

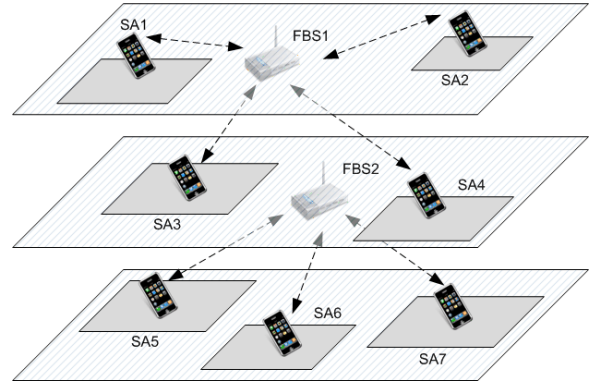


Fig. 1. An illustration of a femtocell network with multiple FBSs and SAs in a multi-floor commercial building. The FBSs are mounted on the ceiling of each floor.

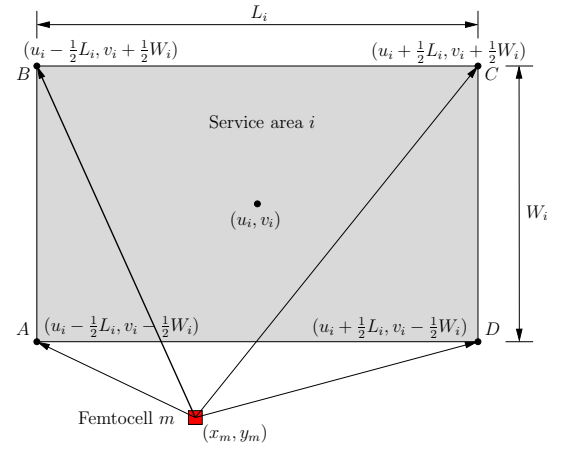


Fig. 2. The projected horizontal distance between FBS m and SA i .

the center of SA i . The length and width of SA i are denoted as L_i and W_i , respectively. Similarly, we use (x_m, y_m, z_m) , $m = 1, \dots, M$, to denote the coordinates of FBS m , which are to be determined.

We first consider the horizontal distance between FBS m and SA i , as shown in Fig. 2. To ensure that FBS m can cover every point in SA i , we define the horizontal distance as the straight line between FBS m and the point in the SA i that is furthest away from FBS m in the projected horizontal space. For example, in Fig. 2, the furthest point in SA i away from FBS m is point C . It is easy to see that, under this definition, the x -axis and y -axis projections are $|x_m - u_i| + \frac{1}{2}L_i$ and $|y_m - v_i| + \frac{1}{2}W_i$, respectively.

Next, we consider the vertical distance. Due to the practical use of building space, FBSs are usually required to be mounted on the ceiling of each floor to avoid being obstructions. Also, due to human height, each handset (HS) is approximately 3 to 4 feet above the ground of each floor. To model this, we further restrict the vertical coordinates w_i and z_m to be integer-valued and in the set $\{1, 2, \dots, F\}$, where F is the maximum number of floors. For example, $w_i = 2$ and $z_m = 3$ represent that SA i and FBS m are on the second floor and the ceiling of the third floor, respectively. We assume that the height of each floor is h . We let η denote the average height of an HS. Then, the vertical distance can be computed as $|(z_m - w_i + 1)h - \eta|$. For example, in Fig. 3, if the FBS is on the second floor and

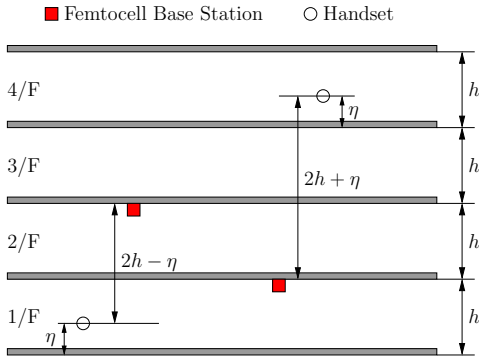


Fig. 3. The vertical distances between femtocell base stations and handsets.

the HS is on the first floor, we have $|(2-1+1)h-\eta| = 2h-\eta$. On the other hand, if the FBS is on the first floor and the HS is on the fourth floor, we have $|(1-4+1)h-\eta| = 2h+\eta$.

Combining the horizontal and vertical distance projections, we can compute the distance between FBS m and SA i , denoted by d_{im} , as:

$$d_{im} = \left[(|x_m - u_i| + \frac{1}{2}L_i)^2 + (|y_m - v_i| + \frac{1}{2}W_i)^2 + |(z_m - w_i + 1)h - \eta|^2 \right]^{\frac{1}{2}}. \quad (1)$$

We let P_{T_i} denote the uplink transmission power of the HS in SA i that is furthest away from its associated FBS (cf. the above definition of the projected horizontal distance). Due to the transmission power limit of an HS, we have $0 \leq P_{T_i} \leq P_{\max}$, $\forall i = 1, 2, \dots, N$, where P_{\max} denotes the maximum transmission power limit for every HS. For simplicity, we assume that the transmission power limit is the same for all HSs. The case where the HSs having heterogeneous transmission power limits can also be easily accommodated in our analytical framework but at the expense of more complex notation.

B. Path Loss Modeling for Commercial Buildings

In commercial building environments, there exist a variety of interior partitions and obstacles. Partitions vary drastically in their physical and electrical characteristics. Due to this complexity, it is difficult to accurately measure and derive a general path loss model. In this paper, we use the following approach to balance accuracy and tractability.

For the path loss within the same floor, we adopt the following equation to model path loss (in dBm) [15]:

$$P_{R_m} = P_{T_i} - L_{d_0} - 10\alpha \log_{10} \left(\frac{d_{im}}{d_0} \right), \quad (2)$$

where P_{R_m} is the received power at FBS m (measured over multiple frames to average out the fast fading effect); P_{T_i} is the transmission power from the point in SA i that is furthest away from FBS m (cf. Fig. 2); d_{im} represents the distance between SA i and FBS m as defined in (1); d_0 is a short reference distance; L_{d_0} represents the signal loss (dB) at distance d_0 ; and α denotes the path loss exponent, indicating the rate at which the signal is attenuated with respect to d_{im} . Since researchers have conducted extensive measurements to

determine α for a large number of partition types (see [15, Table 4.3]), this allows us to use different values of α to model different buildings.

Next, we incorporate the path loss that result from floor separations. We adopt the following model [15]:

$$P_{R_m} = P_{T_i} - L_{d_0} - 10\alpha \log_{10} \left(\frac{d_{im}}{d_0} \right) - L_{FAF}, \quad (3)$$

where L_{FAF} (in dB) denotes the path loss due to the floor attenuation factor (FAF), and where FAF is determined by the external dimensions and materials of the building as well as the construction methods used for the floors and the external surroundings [15], [16], [17]. As a general rule, the FAF between a single floor separation is greater than the incremental attenuation caused by each additional floor [15]. Moreover, FAF approximately follows the following relationship with respect to the number of separating floors [15, Table 4.4]:

$$L_{FAF} = \begin{cases} \Delta_1 + (\varphi - 1)\Delta_a, & \text{if } \varphi \geq 1, \\ 0, & \text{if } \varphi = 0, \end{cases} \quad (4)$$

where Δ_1 represents the FAF for the first floor separation, Δ_a represents the FAF for each additional floor, and φ denotes the number of separating floors.

Converting (3) to a linear scale, we have the following result to model path loss in commercial buildings. We relegate the proof of this result to Appendix A.

Lemma 1. *Under the wireless signal path loss model in (3) and (4) and upon converting P_{R_m} , P_{T_i} , and L_{d_0} to a suitable linear scale, the following relationship holds:*

$$P_{R_m} = \frac{P_{T_i}}{C(z_m, w_i) d_{im}^\alpha \Delta^{|z_m - w_i|}}, \quad \forall i, m, \quad (5)$$

where Δ is a constant that depends on the specific environment; $C(z_m, w_i)$ is a step function that depends on z_m and w_i and has the following structure:

$$C(z_m, w_i) = \begin{cases} C_0, & \text{if } z_m = w_i, \\ C_1, & \text{if } z_m \neq w_i, \end{cases}$$

where C_0 and C_1 are constants that also depend on the specific environment.

C. QoS Requirement Constraints

To reliably decode the i -th HS's transmission at a data rate that satisfies the HS's QoS requirement, it is necessary that the i -th HS's received power level at the FBS should be above a certain threshold value. Let $P_{\min}^{(i)}$ denote the minimum power level. Based on the path loss model in Lemma 1, we have

$$\frac{P_{T_i}}{C(z_m, w_i) d_{im}^\alpha \Delta^{|z_m - w_i|}} \geq P_{\min}^{(i)}, \quad \forall i, m. \quad (6)$$

By rearranging terms and letting

$$A_i(z_m, w_i) \triangleq C(z_m, w_i) P_{\min}^{(i)} = \begin{cases} A_0^{(i)} \triangleq C_0 P_{\min}^{(i)} & \text{if } z_m = w_i, \\ A_1^{(i)} \triangleq C_1 P_{\min}^{(i)} & \text{if } z_m \neq w_i, \end{cases}$$

we can rewrite the QoS constraints in (6) as

$$A_i(z_m, w_i) d_{im}^\alpha \Delta^{|z_m - w_i|} - P_{T_i} \leq 0, \quad \forall i, m. \quad (7)$$

D. FBS Association Modeling

In conventional cellular networks, an SA is usually associated with the nearest base station since the corresponding wireless channel condition is usually the best. In a commercial building environment, however, an optimal FBS association selection becomes more complicated. For each SA, the channel to the nearest FBS may or may not be the best because the nearest FBS could be separated by a floor. From the path loss model in (5), it is not difficult to see that the nearest FBS might actually have a worse path loss because of the FAF effect. Due to this complication, we try not to define a specific rule for FBS association. Instead, we model the FBS association problem as a part of the overall joint FBS placement and power control optimization and let the optimal FBS association be determined by the proposed optimization model. To this end, we first define the following binary variables:

$$\pi_{im} = \begin{cases} 1 & \text{if SA } i \text{ is associated with FBS } m, \\ 0 & \text{otherwise.} \end{cases} \quad (8)$$

Then, the FBS association can be modeled as

$$\sum_{m=1}^M \pi_{im} = 1, \quad \forall i = 1, \dots, N. \quad (9)$$

Due to the above FBS association modeling technique, we need to modify the QoS constraints in (7) as follows:

$$A(z_m, w_i) \pi_{im} d_{im}^\alpha \Delta^{|z_m - w_i|} - P_{T_i} \leq 0, \quad \forall i, m. \quad (10)$$

It can be easily verified that, if $\pi_{im} = 1$ (i.e., if SA i is associated with FBS m), then (10) is identical to the original QoS constraint in (7). Otherwise, if $\pi_{im} = 0$, then (10) reduces to $P_{T_i} \geq 0$, which is trivially valid.

E. Problem Formulation

Based on the foregoing discussion, we are now in a position to study the FBS placement problem in commercial buildings. To prolong the HS battery lives and ensure fairness among all SAs, we can minimize the maximum *uplink* transmission power originating from the SAs, i.e., $\min \{ \max_{i \in \{1, \dots, N\}} P_{T_i} \}$. For easier manipulation, we rewrite the minimax objective function in an equivalent form as: $\min P$, subject to $P \geq P_{T_i}, \forall i = 1, \dots, N$. Incorporating other constraints established earlier, we can formulate the joint FBS placement and power control problem (FPPC) as follows:

FPPC:

$$\text{Min } P \quad (11)$$

$$\text{s.t. } P \geq P_{T_i}, \quad \forall i, \quad (12)$$

$$A_i(z_m, w_i) \pi_{im} d_{im}^\alpha \Delta^{|z_m - w_i|} - P_{T_i} \leq 0, \quad \forall i, m, \quad (13)$$

$$\sum_{m=1}^M \pi_{im} = 1, \quad \forall i, \quad (14)$$

$$d_{im} = \left[\left(|x_m - u_i| + \frac{1}{2} L_i \right)^2 + \left(|y_m - v_i| + \frac{1}{2} W_i \right)^2 + |(z_m - w_i + 1)h - \eta|^2 \right]^{\frac{1}{2}}, \quad \forall i, m, \quad (15)$$

where the decision variables are $[x_m, y_m, z_m]^T, P_{T_i}$, and $\pi_{im}, \forall i, m$. In FPPC, $P_{T_i} \in [0, P_{\max}]$, $\pi_{im} \in \{0, 1\}$, $z_m \in \{1, \dots, F\}$, $x_m \in [0, x_{\max}]$, and $y_m \in [0, y_{\max}]$, where x_{\max} and y_{\max} denote the length and width of the building, respectively.

Observing that FPPC involves binary variables π_{im} and nonconvex constraints in (13) and (15), we have that FPPC is a *mixed-integer nonconvex programming problem* (MINCP), which is NP-hard in general [18]. Also, since (13) is highly unstructured, directly solving FPPC is difficult and no standard optimization tools can be readily applied. In Section III, we first employ a set of novel transformation techniques to reformulate FPPC as an equivalent problem that is much easier to handle. Then, we propose an optimization approach that guarantees finding a global optimal solution. Before concluding this section, we point out that, while the main goal of FPPC is to minimize the uplink transmission powers, a positive side-effect is that the *uplink leakage* (i.e., femto users creating interferences to macro users) is also significantly suppressed due to the decrease in transmission powers.

III. A GLOBAL OPTIMIZATION SOLUTION APPROACH

We first focus on developing the key components to reformulate FPPC as an *equivalent* mixed-integer convex program (MICP) in Section III-A. Then, based on the equivalent MICP, we propose in Section III-B a branch-and-bound (BB) algorithm that employs a convex programming relaxation (CPR) to solve the equivalent problem. Lastly, we discuss a symmetry-defeating strategy in Section III-C to enhance the convergence performance of the BB process.

A. Problem Reformulation

First, we note that the difficulty in solving FPPC stems from the term $A(z_m, w_i) \pi_{im} d_{im}^\alpha \Delta^{|z_m - w_i|}$ in (13) and the nonconvexity in (15). Hence, our ultimate goal is to convert the highly unstructured constraint (13) and the nonconvex constraint (15) into a form that is solvable by standard optimization tools.

Reformulating the Distance Constraint in (15): We first let $\delta_{im} \triangleq d_{im}^2, \forall i, m$, so that (15) can be rewritten as:

$$\delta_{im} = \left(|x_m - u_i| + \frac{1}{2} L_i \right)^2 + \left(|y_m - v_i| + \frac{1}{2} W_i \right)^2 + |(z_m - w_i + 1)h - \eta|^2, \quad \forall i, m. \quad (16)$$

Accordingly, (13) becomes:

$$A(z_m, w_i) \pi_{im} \delta_{im}^{\frac{\alpha}{2}} \Delta^{|z_m - w_i|} - P_{T_i} \leq 0. \quad (17)$$

Now, consider the following result:

Lemma 2. *Constraint (16) can be equivalently replaced by:*

$$\delta_{im} \geq \left(|x_m - u_i| + \frac{1}{2} L_i \right)^2 + \left(|y_m - v_i| + \frac{1}{2} W_i \right)^2 + |(z_m - w_i + 1)h - \eta|^2, \quad \forall i, m. \quad (18)$$

Moreover, the inequality in (18) automatically holds as an equality at an optimal solution.

Proof: Consider FPPC with (13) and (15) respectively replaced by (17) and (18), and suppose that (18) holds as a strict inequality at optimality for some i, m . Then, by decreasing the corresponding values of δ_{im} to make (18) hold as an equality, we still maintain feasibility in (17), and hence retain the optimality of the revised solution. ■

It is not difficult to verify that (18) is now a convex constraint, in contrast with the original nonconvex constraint in (15). However, we note that the right-hand-side (RHS) of (18) involves absolute values, which are non-differentiable and remain cumbersome for designing algorithms. To address this issue, we let $X_{im} \triangleq |x_m - u_i|$ and $Y_{im} \triangleq |y_m - v_i|$. Then, (18) can be rewritten as the following group of constraints:

$$\begin{cases} (X_{im} + \frac{1}{2}L_i)^2 + (Y_{im} + \frac{1}{2}W_i)^2 \\ \quad + (hz_m - ((w_i - 1)h + \eta))^2 - \delta_{im} \leq 0, \\ |x_m - u_i| = X_{im}, \quad |y_m - v_i| = Y_{im}. \end{cases} \quad (19)$$

It can be seen in (19) that the first constraint is a quadratic convex constraint. The second and the third constraints involve absolute value operations, which can be further linearized. For example, based on the same argument as in Lemma 2, we can rewrite the second constraint in (19) as $|x_m - u_i| \leq X_{im}$. This inequality can be further written as $x_m - X_{im} \leq u_i$ and $-x_m - X_{im} \leq -u_i$, both of which are linear constraints. After rearranging terms, we arrive at the following result:

Lemma 3. *The distance constraint (15) can be convexified as:*

$$\begin{cases} (X_{im} + \frac{1}{2}L_i)^2 + (Y_{im} + \frac{1}{2}W_i)^2 \\ \quad + (hz_m - ((w_i - 1)h + \eta))^2 - \delta_{im} \leq 0, \\ x_m - X_{im} \leq u_i, \quad -x_m - X_{im} \leq -u_i, \\ y_m - Y_{im} \leq v_i, \quad -y_m - Y_{im} \leq -v_i. \end{cases} \quad (20)$$

Reformulating the Minimum Received Power Constraint

in (13): Now, we reformulate (13), which is the most cumbersome relationship in FPPC. Recall that we have restated (13) as (17) by a change of variables. Now, we linearize (17) with respect to the binary variables π_{im} . To this end, we have the following lemma:

Lemma 4. *Constraint (13) is equivalent to the following alternative representation:*

$$A(z_m, w_i) \delta_{im}^{\frac{\alpha}{2}} \Delta^{|z_m - w_i|} (1 - \pi_{im}) U_{im} - P_{T_i} \leq 0, \forall i, m, \quad (21)$$

where U_{im} is some upper bound for $A_i(z_m, w_i) \delta_{im}^{\frac{\alpha}{2}} \Delta^{|z_m - w_i|}$.

Proof: Lemma 4 can be easily verified as follows. If $\pi_{im} = 1$, then (21) is equivalent to the original constraint in (17). Otherwise, if $\pi_{im} = 0$, then we have $A(z_m, w_i) \delta_{im}^{\frac{\alpha}{2}} \Delta^{|z_m - w_i|} - U_{im} \leq 0 \leq P_{T_i}$, which is trivially valid. ■

In Lemma 4, a valid value for the upper bound U_{im} can be chosen as

$$U_{im} \triangleq P_{\min, m}^{(\sigma, \beta)} \max\{C_0, C_1\} (\delta_{im}^U)^{\frac{\alpha}{2}} \Delta^{\max\{w_i - 1, F - w_i\}}, \quad (22)$$

where δ_{im}^U is an upper bound for δ_{im} . Recalling that x_{\max} , y_{\max} , and F are the maximum length, width, and number of

floors of the building, we can compute δ_{im}^U in (22) as:

$$\begin{aligned} \delta_{im}^U &= \max\{(u_i + \frac{1}{2}L_i)^2, (x_{\max} - u_i + \frac{1}{2}L_i)^2\} \\ &\quad + \max\{(v_i + \frac{1}{2}W_i)^2, (y_{\max} - v_i + \frac{1}{2}W_i)^2\} \\ &\quad + \max\{((2 - w_i)h - \eta)^2, ((F - w_i + 1)h - \eta)^2\}. \end{aligned}$$

Next, to further simplify (21), we introduce two new variables $\nu_{im} \triangleq \delta_{im}^{\frac{\alpha}{2}}$ and $\mu_{im} \triangleq \Delta^{|z_m - w_i|}$ and rewrite (21) as the following three constraints:

$$\begin{cases} A(z_m, w_i) \nu_{im} \mu_{im} - (1 - \pi_{im}) U_{im} - P_{T_i} \leq 0, \forall i, m, \\ \nu_{im} = \delta_{im}^{\frac{\alpha}{2}}, \quad \forall i, m, \\ \mu_{im} = \Delta^{|z_m - w_i|}, \quad \forall i, m. \end{cases} \quad (23)$$

Now, consider the nonconvex constraint $\nu_{im} = \delta_{im}^{\frac{\alpha}{2}}$ in (23). We can convexify this constraint as

$$\nu_{im} \geq \delta_{im}^{\frac{\alpha}{2}}, \quad \forall i, m, \quad (24)$$

following the same argument as in Lemma 2. Note that the inequality constraint in (24) is now convex since $\alpha \geq 2$.

The next nonconvex constraint in (23) is $\mu_{im} = \Delta^{|z_m - w_i|}$. Since z_m is integer-valued on $\{1, \dots, F\}$, we can rewrite it using the following equivalent binary representation:

$$z_m = \sum_{k=1}^F k \lambda_{mk}, \quad \forall m, \quad (25)$$

where λ_{mk} is binary (i.e., $\lambda_{mk} \in \{0, 1\}$, $\forall m, k$) and satisfies

$$\sum_{k=1}^F \lambda_{mk} = 1, \quad \forall m. \quad (26)$$

As a result, it is easy to verify that $\mu_{im} = \Delta^{|z_m - w_i|}$ is equivalent to the following *linear* constraint in λ_{mk} -variables:

$$\mu_{im} = \sum_{k=1}^F \lambda_{mk} \Delta^{|k - w_i|}, \quad \forall i, m. \quad (27)$$

With (27), we can further simplify the first constraint in (23) into an expression that only involves binary variables instead of general integer variables. Substituting (27) into the first constraint in (23), the latter becomes:

$$A(z_m, w_i) \sum_{k=1}^F \Delta^{|k - w_i|} \nu_{im} \lambda_{mk} - (1 - \pi_{im}) U_{im} - P_{T_i} \leq 0. \quad (28)$$

Recall that $A(z_m, w_i)$ is equal to A_0 if $z_m = w_i$; or equals A_1 if $z_m \neq w_i$. Thus, (28) can be further written as

$$A_1 \sum_{k=1, k \neq w_i}^F \Delta^{|k - w_i|} \nu_{im} \lambda_{mk} + A_0 \nu_{im} \lambda_{mw_i} - (1 - \pi_{im}) U_{im} - P_{T_i} \leq 0. \quad (29)$$

So far, we have converted the highly unstructured expression in (13) to an expression in (29) that is linear in the binary variables π_{im} but has *bilinear* terms $\nu_{im} \lambda_{mk}$. Now, we are in a position to apply the special-structured *Reformulation Linearization Technique* (RLT) of Sherali *et al.* [19] to linearize the bilinear terms $\nu_{im} \lambda_{mk}$ in (29). First, we let

$$g_{imk} \triangleq \nu_{im} \lambda_{mk}, \quad \forall i, m, k. \quad (30)$$

Then, (29) can be linearized as

$$A_1 \sum_{k=1, k \neq w_i}^F \Delta^{|k-w_i|} g_{imk} + A_0 g_{imw_i} - (1 - \pi_{im}) U_{im} - P_{T_i} \leq 0. \quad (31)$$

Now, the RLT task boils down to linearizing the expression $g_{imk} = \nu_{im} \lambda_{mk}$, which leads to the following result:

Theorem 1. *Given (26) with $\lambda_{mk} \in \{0, 1\}$, $\forall m, k$, the bilinear equation $g_{imk} = \nu_{im} \lambda_{mk}$ in (30) holds if and only if*

$$g_{imk} - \nu_{im}^U \lambda_{mk} \leq 0, \quad g_{imk} \geq 0, \quad \forall i, m, k, \quad (32)$$

$$\sum_{k=1}^F g_{imk} - \nu_{im} = 0, \quad \forall i, m, \quad (33)$$

where ν_{im}^U denotes an upper bound for ν_{im} . Moreover, the special-structured RLT relaxation in (32) and (33) yields the convex hull of the original bilinear constraint (30).

Proof: We first show the ‘‘only if’’ part. Since ν_{im} is non-negative and upper bounded and λ_{mk} is binary, we have

$$\nu_{im} \geq 0, \quad \nu_{im} - \nu_{im}^U \leq 0, \quad \text{and} \quad \lambda_{mk} \geq 0, \quad (34)$$

in addition to (26). From the inequalities in (34), we derive the following two so-called bound-factor constraints: $\nu_{im} \lambda_{mk} \geq 0$, and $(\nu_{im} - \nu_{im}^U) \lambda_{mk} \leq 0$, which, upon applying the substitution (30), yield: $g_{imk} \geq 0$ and $g_{imk} - \nu_{im}^U \lambda_{mk} \leq 0$, i.e., the expressions in (32). Furthermore, multiplying both sides of (26) by ν_{im} and using (30), we obtain $\sum_{k=1}^F g_{imk} - \nu_{im} = 0$, $\forall i, m$, i.e., the expression in (33). This completes the proof of the ‘‘only if’’ part of the theorem.

Conversely, if $\lambda_{mk} = 0$, then (32) implies that $g_{imk} = 0 = \nu_{im} \cdot 0 = \nu_{im} \lambda_{mk}$. On the other hand, when $\lambda_{mk} = 1$, it follows from (26) that $\lambda_{mk'} = 0, \forall k' \neq k$. As above, we have $g_{imk'} = 0, \forall k' \neq k$. Thus, we obtain that $g_{imk} = \nu_{im} = \nu_{im} \cdot 1 = \nu_{im} \lambda_{mk}$, using (33) along with $g_{imk'} = 0, \forall k' \neq k$. This completes the proof of the ‘‘if’’ part of the theorem. The final statement of the theorem follows from [19]. ■

Using Theorem 1 and putting together all the previous derivations, we obtain the following equivalent reformulation for FPPC (denoted as R-FPPC):

R-FPPC:

Min P

- s.t. a) RLT reformulation for minimum received power constraints: (12), (24), (25), (26), (31), (32), (33),
- b) Distance reformulation constraints: (20),
- c) FBS association constraint: (14).

In R-FPPC, all constraints are either linear or convex, and so R-FPPC is a *mixed-integer convex program* (MICP), which is readily solvable using a branch-and-bound (BB) framework, where lower bounds are computed using the continuous convex programming relaxation (CPR) of R-FPPC. More specifically, due to (14) and (26) within the model, the CPR of R-FPPC is obtained by replacing the binary restrictions on π and λ with non-negative constraints. In Section III-B, we will present in detail the algorithmic framework of BB/CPR.

B. A Solution Procedure Based on a Branch-and-Bound Framework and Convex Programming Relaxations (BB/CPR)

The basic idea of BB/CPR is that, by using the CPR, we can efficiently compute a global lower bound, LB , for R-FPPC. This relaxation solution either yields a feasible solution to R-FPPC or, if not feasible, it can be used as a starting point for a local search to find a feasible solution. This feasible solution then serves to provide a global upper bound, UB , and an incumbent solution to R-FPPC. The BB process proceeds by tightening LB and UB through a series of partitions over the problem domain, and terminates when $UB \leq (1 + \epsilon)LB$ is satisfied, where $\epsilon > 0$ is some desired approximation error. It follows from [20], [21], [22] that, if the domain of the CPR is compact, the BB/CPR process is guaranteed to converge to a global optimal solution. This condition clearly holds in FPPC. We refer readers to [20], [21], [22] for more details about the proof of the convergence guarantee.

The detailed BB/CPR process for R-FPPC works as follows. Recall that we have substituted g_{imk} -variables in (30) to represent the nonconvex bilinear terms in R-FPPC. Since these bilinear terms involve a product with a binary variable, from Theorem 1, we know that Eq. (30) will hold as long as the λ -variables are binary-valued. Therefore, for R-FPPC, we only need to branch on the binary variables (π, λ) . Specifically, we select a binary π - or λ -variable and branch on the dichotomy of its value being 0 or 1. After branching, the original problem (denoted as P_1 in Fig. 4(a)) having the lower bound $LB_1 = LB$ is divided into two new subproblems (denoted as P_2 and P_3 in Fig. 4(b)). Then, we solve the corresponding CPRs for P_2 and P_3 , and thereby obtain LB_2 and UB_2 for P_2 , and LB_3 and UB_3 for P_3 . Since the domains for P_2 and P_3 are both more restricted than that for P_1 , we must have $\min\{LB_2, LB_3\} \geq LB_1$. Then, the global lower bound is updated to $LB = \min\{LB_2, LB_3\}$ and the global upper bound is updated to $UB = \min\{UB, UB_2, UB_3\}$. The incumbent solution is also updated in case an improvement results. Now, we have a smaller gap between LB and UB . If $UB \leq (1 + \epsilon)LB$, the BB process is terminated. Otherwise, we choose a subproblem that has the minimum lower bound (e.g., P_3 in Fig. 4(b)) and perform a further partition. In the next iteration, as shown in Fig. 4(c), P_3 is partitioned into P_4 and P_5 . Upon solving the CPRs for P_4 and P_5 , respectively, we have two sets of lower and upper bounds (LB_4, UB_4) and (LB_5, UB_5) . We note in P_5 (see Fig. 4(c)) that $(1 + \epsilon)LB_5 > UB$. This means that a further partition of P_5 is unnecessary. As such, we can discard P_5 (i.e., fathom it) from the problem list. After the partition of P_3 is done, the global lower bound becomes $LB = \min\{LB_2, LB_4, LB_5\}$, which is LB_2 in this case (see Fig. 4(c)). This process repeats until $UB \leq (1 + \epsilon)LB$. We summarize the BB/CPR procedure in Algorithm 1.

Finally, we point out that the BB/CPR approach can be used to determine an appropriate value of M to ensure coverage. For a given network, we can start from a small value, say $M = 1$ (for the case of finding a minimal M value). If M is too small to ensure coverage, BB/CPR will detect the infeasibility of the underlying problem. Then, we can iteratively double M

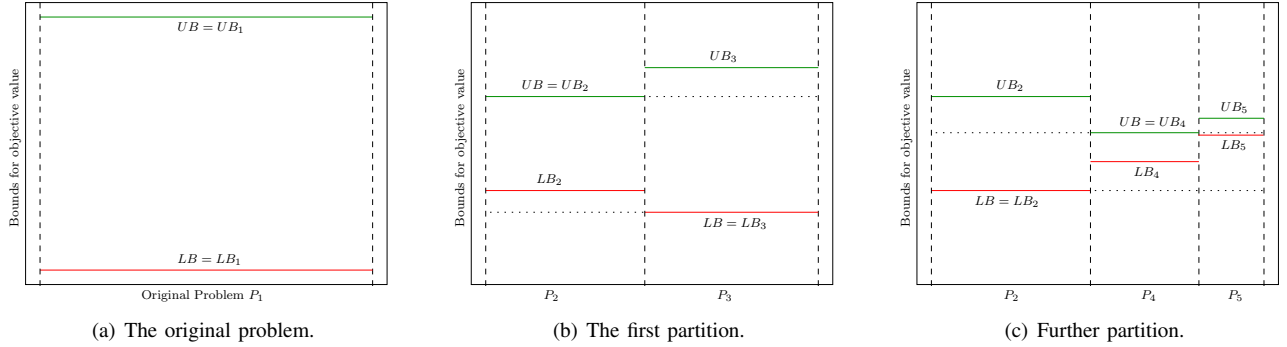


Fig. 4. Illustration of the branch-and-bound solution framework.

Algorithm 1 BB/CPR Solution Procedure

Initialization:

1. Let the optimal solution $\psi^* = \emptyset$ and the initial upper bound $UB = \infty$.
2. Let the initial problem list contain only the original problem, denoted by P_1 .
3. Construct and solve the convex programming relaxation for P_1 . Denote the solution to this relaxation as ψ_1 and its objective value as the lower bound LB_1 .

Main Loop:

4. Select a problem P_z that has the smallest lower bound (designated as LB) among all the problems in the problem list.
 5. Find, if necessary, a feasible solution ψ_z via a local search algorithm for P_z . Denote the objective value of ψ_z by UB_z .
 6. If $UB_z < UB$, then let $\psi^* = \psi_z$ and $UB = UB_z$. If $UB \leq (1 + \epsilon)LB$, then stop with the $(1 + \epsilon)$ -optimal solution ψ^* ; else, remove all problems $P_{z'}$ having $(1 + \epsilon)LB_{z'} \geq UB$ from the problem list.
 7. Select a binary π - or λ -variable and branch on the dichotomy of its values being 0 or 1.
 8. Remove the selected problem P_z from the problem list, construct two new problems P_{z1} and P_{z2} based on the foregoing branching step.
 9. Compute two new lower bounds LB_{z1} and LB_{z2} by solving the convex programming relaxations of P_{z1} and P_{z2} , respectively.
 10. If $UB > (1 + \epsilon)LB_{z1}$ then add Problem P_{z1} to the problem list. If $UB > (1 + \epsilon)LB_{z2}$ then add Problem P_{z2} to the problem list.
 11. If the problem list is empty, stop with the $(1 + \epsilon)$ -optimal solution ψ^* . Otherwise, go to Step 4.
-

and repeat BB/CPR until the problem becomes feasible. Note that to determine the minimal value of M (denoted as M^*), we can then perform a bisection search on the final deduced interval (of complexity $O(\log(M^*))$).

C. Convergence Speedup: A Symmetry-Defeating Approach

In Section III-B, we have proposed a global optimization technique based on BB/CPR to solve R-FPPC. Here, we further investigate the possibility of tightening the R-FPPC model to speed up the BB convergence process. Upon a closer look at R-FPPC, we can see that there exists a *symmetry* with respect to the FBSs in the model. For example, if we have a case of three FBSs indexed by 1, 2, and 3, and if the optimal locations are, say, $(50.2, 26.1, 2)$, $(75.2, 39.1, 2)$, and $(18.4, 56.3, 3)$, then any permutation of the FBS indices assigned to the above locations would yield an identical optimal solution. For example, the solution $(x_1, y_1, z_1) = (50.2, 26.1, 2)$, $(x_2, y_2, z_2) = (75.2, 39.1, 2)$, and $(x_3, y_3, z_3) = (18.4, 56.3, 3)$ is essentially not different from, say, $(x_3, y_3, z_3) = (50.2, 26.1, 2)$, $(x_2, y_2, z_2) = (75.2, 39.1, 2)$, and $(x_1, y_1, z_1) = (18.4, 56.3, 3)$. This phe-

nomenon is due to the fact that the FBSs are *indistinguishable* objects by nature. As a result, when the network size is large, the BB procedure could be hopelessly mired by being forced to explore and discard symmetric reflections of various solutions during the search process [23]. To defeat this symmetry, we introduce the following *lexicographic order constraint*:

$$(z_m, x_m, y_m) \stackrel{L}{\geq} (z_{m+1}, x_{m+1}, y_{m+1}), m = 1, \dots, M - 1, (35)$$

where $\stackrel{L}{\geq}$ denotes the ‘‘lexicographically greater than or equal to’’ order. Under this lexicographic order constraint, the only feasible indices assignment of the previous example is: $(x_1, y_1, z_1) = (18.4, 56.3, 3)$, $(x_2, y_2, z_2) = (75.2, 39.1, 2)$, and $(x_3, y_3, z_3) = (50.2, 26.1, 2)$, rather than $3! = 6$ equally valid assignments. Note that in (35), we place the most emphasis on the vertical coordinate z_m , which is integer-valued, by making it the first element in the 3-tuple. We will explain this further after introducing a mathematical model for the lexicographic order constraint in (35). To model (35), we let $U_{\max} \equiv \max\{x_{\max}, y_{\max}, F\}$. Then, we have the following result and its proof is relegated to Appendix B.

Proposition 1. *Suppose that the unequal x -coordinates between locations of FBSs at optimality differ by at least $\bar{\epsilon} > 0$. Then, the constraint in (35) holds if and only if*

$$U^2 z_m + U x_m + y_m \geq U^2 z_{m+1} + U x_{m+1} + y_{m+1}, (36)$$

where $m = 1, \dots, M - 1$ and the parameter U is defined as $U \triangleq \max\{\frac{U_{\max}}{\bar{\epsilon}}, U_{\max} + 1\}$.

It is worth pointing out that there could be multiple ways to model (35). Our choice of the function in (36) is motivated by [23]. The key difference to [23] is that, in this paper, x_m and y_m are real variables, whereas in [23], all variables are integer-valued. This difference leads to a difference definition of the parameter U and the proof becomes more involved.

Note that when selecting the value of U in Proposition 1, we need the knowledge of $\bar{\epsilon}$ (i.e., a lower bound of the minimal difference between unequal x -values in the set of optimal solutions), which is unknown at the beginning of the BB process. Fortunately, this issue is not critical because we are not required to guarantee the lexicographic order, but only need to impose a constraint that would tend to respect this relationship. Hence, we could choose some small value for $\bar{\epsilon}$

TABLE I
THE COORDINATES AND SIZES OF SAs IN THE NETWORK IN FIG. 5.

SA	1	2	3	4	5	6	7	8	9	10
u_i	12.7	43.1	73.7	94.4	20.4	25.9	61.1	87.1	14.0	35.7
v_i	13.7	0.2	14.3	4.9	20.1	16.8	24.0	25.0	30.2	36.0
w_i	2	3	3	2	2	1	2	1	1	1
L_i	19.4	14.4	18.5	11.1	16.1	18.8	17.7	14.9	16.5	16.6
W_i	11.6	0.3	10.2	8.5	1.4	10.1	10.3	8.4	10.2	9.6

SA	11	12	13	14	15	16	17	18	19	20
u_i	70.1	82.2	15.1	40.0	57.3	97.9	65.1	51.1	83.6	5.9
v_i	40.3	40.3	59.1	59.2	58.6	45.8	52.4	43.8	24.0	40.9
w_i	3	2	1	1	2	3	2	3	3	3
L_i	14.4	19.4	17.1	14.5	19.3	4.1	18.1	16.4	19.2	11.9
W_i	10.0	8.5	1.8	1.7	2.9	9.4	9.4	10.1	9.1	10.1

TABLE II
THE OPTIMAL FBS LOCATIONS FOR THE NETWORK IN FIG. 5.

	No Symmetry-Defeating			Symmetry-Defeating		
	x	y	z	x	y	z
FBS1	57.2227	57.1399	3	57.2266	57.1679	3
FBS2	52.4335	27.8875	2	52.4577	27.4921	2
FBS3	60.4158	25.0149	1	60.4158	25.0151	1

(e.g., $\bar{\epsilon} \ll 1$) such that it would defeat most of the inherent symmetry with high probability. Such an approach would still assist in significantly curtailing the enumeration effort.

Also, from the proof in Appendix B, we can see that our choice of U guarantees the lexicographic order in the z -variables regardless of the value of $\bar{\epsilon}$. This is because z_m is integer-valued, implying that unequal z -values differ by at least 1. This explains why we place the most emphasis on z_m .

IV. NUMERICAL RESULTS

In this section, we conduct numerical studies for the proposed BB/CPR algorithm and the symmetry-defeating strategy. We first use a 20-SA network in a 3-story building as an example. The building's length, width, and per-floor height are 100, 60, and 3 meters, respectively. The length and width of all SAs are randomly generated and uniformly distributed in the intervals $[0, 20]$ and $[0, 16]$ (in meter), respectively (the parameters 20 and 16 are chosen for the purpose of better visibility in Fig. 5, and they could be set to more practical values for specific buildings in practice). The coordinates and size of each SA are shown in Table I. We plan to place three FBSs to serve this network. The maximum transmission power limit and minimum received power threshold for each HS are 1 W and -100 dBm, respectively. The path loss exponent is 4. Under BB/CPR and no symmetry-defeating, the maximum transmission power is minimized to 0.1144 W, and the optimal FBS locations are shown in the left half of Table II. The optimal FBS placement and FBS-SA association relationship are shown in Fig. 5. As expected, due to FAF, not all SAs are associated with their nearest FBSs. For example, SA14 is not associated with FBS3, which is the nearest but separated by two floors. Instead, it is associated with FBS1, which is on the same floor but much further away compared to FBS3.

Now, we use the same network in Fig. 5 to demonstrate the efficacy of the symmetry-defeating strategy. The convergence speed comparison is shown in Table III. Under symmetry-defeating, the BB process converges in 554 seconds after

TABLE III
THE EFFECT OF SYMMETRY-DEFEATING ON THE SPEED OF CONVERGENCE.

Without Symmetry-Defeating		With Symmetry-Defeating	
BB Iter.	Time (sec)	BB Iter.	Time (sec)
8498	2445	3189	554

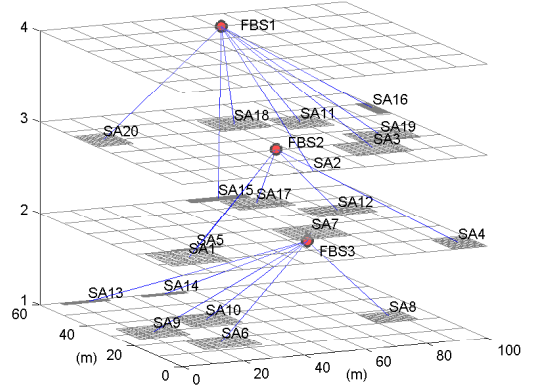


Fig. 5. The optimal FBS placement and FBS-SA association relationship for a 20-SA network.

exploring 3189 BB nodes. The BB convergence process is illustrated in Fig. 6. Interestingly, we note that the local search did not identify any integer feasible solution (global upper bound) until after 1735 BB iterations, more than half way through the BB process. However, the global upper bound improves much more quickly, playing a key role in the overall convergence time of the BB process. In contrast, without the symmetry-breaking strategy, it takes 2445 seconds (exploring 8498 BB nodes) for the BB process to converge, which is substantially longer. Also, under symmetry-defeating, the optimal objective value is again found to be 0.1144 W, exactly the same as that without this strategy. As expected, adding the symmetry-defeating constraints does not affect the optimal objective value. The optimal FBS locations obtained by using symmetry-defeating are shown in the right half of Table II. Compared to the solutions obtained without this technique, we can see that the differences are negligible, i.e., the symmetry-defeating strategy does not affect the optimality of the solution. Also, we can see that these solutions are lexicographically ordered as required. This corroborates with our analysis that (36) enforces the lexicographic ordering.

Next, we test the robustness of BB/CPR by studying the scaling of the convergence time with respect to the numbers of SAs and FBSs. The corresponding results are shown in Fig. 7 and Fig. 8, respectively. In the simulations, the building parameters and wireless channel settings are the same as in the previous example. Each data point in Fig. 7 and Fig. 8 is obtained by averaging over 50 randomly generated network instances. In Fig. 7, the number of FBSs is three and we increase the number of SAs from 11 to 25. In Fig. 8, the number of SAs is 10 and we increase the number of FBSs from three to six. In both cases, the convergence time of the global optimization approach increases rather slowly. This observation is important because the smooth scaling of the convergence time demonstrates the robustness and efficacy of

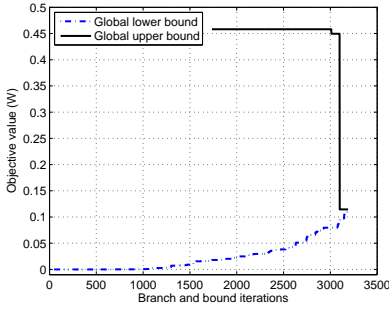


Fig. 6. The convergence process of BB/CPR for the network example in Fig. 5.

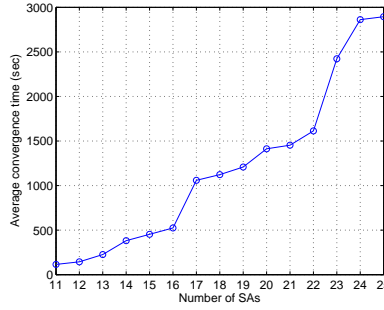


Fig. 7. The scaling of convergence time with respect to the number of SAs. The number of FBSs is three. Each data point is obtained by averaging over 50 randomly generated network instances.

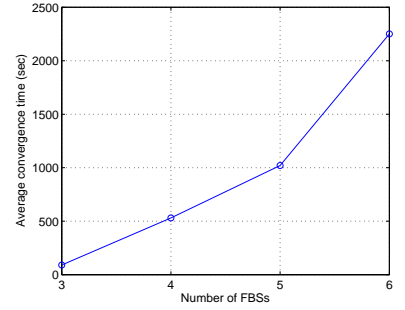


Fig. 8. The scaling of convergence time with respect to the number of FBSs. The number of SAs is 20. Each data point is obtained by averaging over 50 randomly generated network instances.

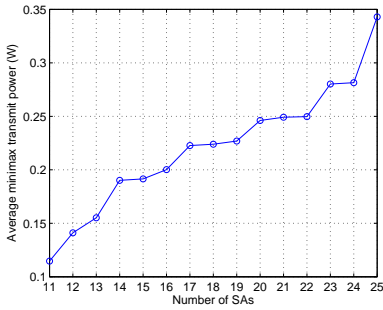


Fig. 9. The scaling of minimized maximum transmitted power with respect to the number of SAs. The number of FBSs is three. Each data point is obtained by averaging over 50 randomly generated network instances.

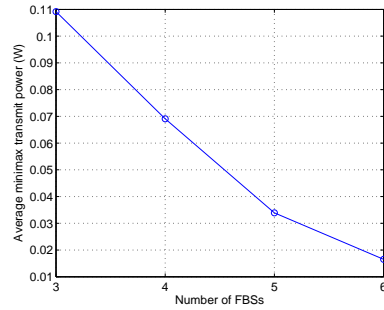


Fig. 10. The scaling of minimized maximum transmitted power with respect to the number of FBSs. The number of SAs is 10. Each data point is obtained by averaging over 50 randomly generated network instances.

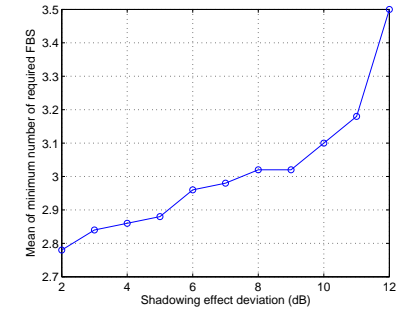


Fig. 11. The scaling of average minimum required number of FBSs with respect to the shadowing effect deviation. Each data point is obtained by averaging over 50 randomly generated network instances.

our proposed symmetry-defeating strategy.

We also test the scaling of the objective value (minimum of the maximal transmission power) with respect to the numbers of SAs and FBSs, and the results are shown in Fig. 9 and Fig. 10, respectively. In these simulations, all building and wireless channel settings remain the same. In Fig. 9, the number of FBSs is three and we increase the number of SAs from 11 to 25. In Fig. 10, the number of SAs is 10 and we increase the number of FBSs from three to six. Again, each data point in Fig. 9 and Fig. 10 is averaged over 50 randomly generated network instances. It can be seen that the objective value gradually increases with respect to the number of SAs. This makes intuitive sense because, as the number of SAs increases, the distance between the furthest SA to its associated FBS also tends to increase. Furthermore, the transmission power increases exponentially with respect to the distance, hence the result in Fig. 9. On the other hand, we can see from Fig. 10 that the objective value decreases with respect to the number of FBSs. This also makes sense since, with more FBSs, we have greater freedom and possibility to place the FBSs in close proximity to the SAs, which significantly reduces the transmission power from each SA.

As mentioned earlier, the proposed BB/CPR algorithm can also be used to determine the minimum required number of FBSs to ensure network coverage, which is also an important question encountered in practical network design. As an ex-

ample, we study here how the minimum required number of FBSs changes as the wireless channel quality varies. Again, the sizes of the buildings used in this simulation remain the same as before. The path loss exponent α is set to 4 and we vary the shadowing effect deviation from 2 dB to 12 dB (i.e., channels fluctuate more and more), which leads to an increase in P_{\min} under a fixed outage probability threshold (set to 0.5% in our simulations). The results are demonstrated in Fig. 11, where each point (corresponding to one channel setting) is obtained by averaging over 50 randomly generated network instances. We can see that when the deviation varies from 2 dB to 12 dB, the average minimum required number of FBSs increases from 2.78 to 3.50.

V. CONCLUSION

In this paper, we investigated the joint femtocell base station (FBS) placement and power control optimization problem in commercial buildings in order to prolong the battery lives of mobile handsets. This problem is challenging due to the impact of the structure of the commercial building on wireless communication channels. To solve this problem, we first formulated a mathematical model to capture the unique features of commercial buildings. Starting with this model, we applied a set of novel transformation strategies to reformulate the problem as a mixed-integer convex program (MICP). This enabled us to design a suitable branch-and-bound optimization

algorithm based on the convex programming relaxation of the reformulated MICP, which *guarantees* finding a global optimal solution. To further enhance the convergence time performance, we proposed a lexicographic ordering strategy that defeats the inherent symmetry in the MICP problem. Our numerical results indicated that the global optimization approach and the symmetry-defeating strategy work well for practical femtocell networks in commercial buildings. The results in this paper offer both important analytical tools and practical insights that enhance our understanding of femtocells deployments in commercial building environments. We note that femtocell placement in commercial buildings is an important and yet under-explored area and there remain many open problems. Possible future directions include the study of joint spectral management and placement optimization problems, and the study of combining FBS placement with multiple-antenna systems and downlink power control in order to tackle the coverage and leakage problem in the downlink.

APPENDIX A PROOF OF LEMMA 1

Combining (2) and (4) and noting that the number of floors between the i -th SA and the m -th FBS is $|z_m - w_i|$, we obtain that (in dBm):

$$P_{R_m} = \begin{cases} P_{T_i} - L_{d_0} - 10\alpha \log_{10} \left(\frac{d_{im}}{d_0} \right), & \text{if } z_m = w_i, \\ P_{T_i} - L_{d_0} - 10\alpha \log_{10} \left(\frac{d_{im}}{d_0} \right) \\ - \Delta_1 - (|z_m - w_i| - 1)\Delta_a, & \text{if } z_m \neq w_i. \end{cases}$$

This implies that, after converting each of P_{R_m} , P_{T_i} , and L_{d_0} to a linear scale (i.e., letting $y = 10^{\frac{x}{10}}$, where x and y are in dBm and the linear scale, respectively), we have

$$P_{R_m} = \begin{cases} \frac{P_{T_i}}{L_{d_0}(d_{im}/d_0)^\alpha}, & \text{if } z_m = w_i, \\ \frac{P_{T_i}}{L_{d_0}(d_{im}/d_0)^\alpha 10^{(\Delta_1/10)} 10^{((|z_m - w_i| - 1)\Delta_a/10)}}, & \text{if } z_m \neq w_i. \end{cases}$$

Then, the result in (5) follows by letting $C_0 = L_{d_0} d_0^{-\alpha}$, $C_1 = L_{d_0} d_0^{-\alpha} 10^{(\Delta_1 - \Delta_a)/10}$, and $\Delta = 10^{\Delta_a/10}$. \square

APPENDIX B PROOF OF PROPOSITION 1

We first prove the ‘‘only if’’ part. Suppose that $(z_m, x_m, y_m) \stackrel{L}{\geq} (z_{m+1}, x_{m+1}, y_{m+1})$. Note that if $(z_m, x_m, y_m) \stackrel{L}{=} (z_{m+1}, x_{m+1}, y_{m+1})$, then (36) trivially holds. If the lexicographic inequality is strict, then it implies that one of the following three cases is true: 1) $z_m > z_{m+1}$; 2) $z_m = z_{m+1}$ and $x_m > x_{m+1}$; or 3) $z_m = z_{m+1}$, $x_m = x_{m+1}$, and $y_m > y_{m+1}$. Consider the first case, i.e., $z_m > z_{m+1}$. Since z_m is integer-valued, $z_m > z_{m+1}$ is equivalent to $z_m \geq z_{m+1} + 1$. Thus, we have

$$\begin{aligned} & (U^2 z_m + U x_m + y_m) - (U^2 z_{m+1} + U x_{m+1} + y_{m+1}) \\ &= U^2 (z_m - z_{m+1}) + (U x_m + y_m) - (U x_{m+1} + y_{m+1}) \\ &\stackrel{(a)}{\geq} U^2 - U_{\max}(U + 1) = U(U - U_{\max}) - U_{\max} \\ &\stackrel{(b)}{\geq} U - U_{\max} \stackrel{(c)}{\geq} 1 > 0, \end{aligned}$$

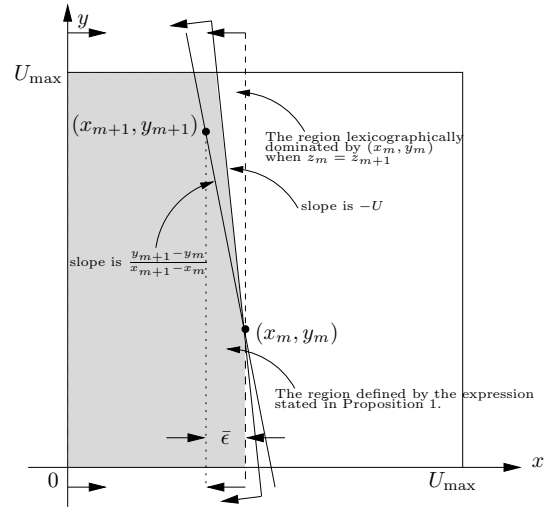


Fig. 12. Geometric insights of (38) under the case where $z_m = z_{m+1}$, $x_m > x_{m+1}$, and $y_m < y_{m+1}$.

where inequality (a) follows from $z_m - z_{m+1} \geq 1$, $U x_m + y_m \geq 0$, and $x_m, y_m \leq U_{\max}$; and inequalities (b) and (c) follow from $U - U_{\max} = \max\{\frac{U_{\max}}{\epsilon}, U_{\max} + 1\} - U_{\max} \geq U_{\max} + 1 - U_{\max} = 1$.

In the second case (i.e., $z_m = z_{m+1}$, $x_m > x_{m+1}$), we have

$$\begin{aligned} & (U^2 z_m + U x_m + y_m) - (U^2 z_{m+1} + U x_{m+1} + y_{m+1}) \\ &= U(x_m - x_{m+1}) + (y_m - y_{m+1}). \end{aligned} \quad (37)$$

Note that $U(x_m - x_{m+1}) > 0$ since $x_m > x_{m+1}$. Hence, if $y_m \geq y_{m+1}$, (37) is positive and we are done. On the other hand, if $y_m < y_{m+1}$, then in order for (37) to be non-negative, U must satisfy:

$$U \geq -\frac{y_{m+1} - y_m}{x_{m+1} - x_m}. \quad (38)$$

The geometrical insight of (38) is illustrated in Fig. 12. In the second case where $z_m = z_{m+1}$ and $x_m > x_{m+1}$, the region lexicographically dominated by (x_m, y_m) can be represented by the subspace between $x < x_m$ and $x \geq 0$. In the case where $x_m > x_{m+1}$ and $y_m < y_{m+1}$, the point (x_{m+1}, y_{m+1}) is located ‘‘northwest’’ to (x_m, y_m) . Also, the region defined by (36) is the shaded area as shown in Fig. 12. It can be seen that in order for the region defined by (36) to cover (x_{m+1}, y_{m+1}) , the slope $-U$ must be less than or equal to the slope of the straight line defined by (x_m, y_m) and (x_{m+1}, y_{m+1}) , i.e., $-U \leq \frac{y_{m+1} - y_m}{x_{m+1} - x_m}$. This is identical to the condition in (38).

Moreover, from the definition of $\bar{\epsilon}$, we have $0 < \bar{\epsilon} \leq x_m - x_{m+1}$. Then, we can derive a valid upper bound for $-\frac{y_{m+1} - y_m}{x_{m+1} - x_m}$ as follows:

$$\frac{y_{m+1} - y_m}{-(x_{m+1} - x_m)} \leq \frac{y_{m+1}}{x_m - x_{m+1}} \leq \frac{U_{\max}}{x_m - x_{m+1}} \leq \frac{U_{\max}}{\bar{\epsilon}}.$$

Hence, choosing $U = \frac{U_{\max}}{\bar{\epsilon}}$ is sufficient for (38) to hold.

In the last case, i.e., $z_m = z_{m+1}$, $x_m = x_{m+1}$, and $y_m > y_{m+1}$, we simply have

$$(U^2 z_m + U x_m + y_m) - (U^2 z_{m+1} + U x_{m+1} + y_{m+1}) > 0.$$

Hence, Eq. (36) again holds true.

Conversely, suppose that Eq. (36) is satisfied but on the contrary we have $(z_{m+1}, x_{m+1}, y_{m+1}) \stackrel{L}{>} (z_m, x_m, y_m)$ holds. Then, following the discussions in the “only if” part, we would have $U^2 z_{m+1} + U x_{m+1} + y_{m+1} > U^2 z_m + U x_m + y_m$, a contradiction. \square

REFERENCES

- [1] V. Chandrasekhar, J. G. Andrews, and A. Gatherer, “Femtocell networks: A survey,” *IEEE Commun. Mag.*, vol. 46, no. 9, pp. 59–67, Sep. 2008.
- [2] R. Y. Kim, J. S. Kwak, and K. Etemad, “WiMAX femtocell: Requirements, challenges, and solutions,” *IEEE Commun. Mag.*, vol. 47, no. 9, pp. 84–91, Sep. 2009.
- [3] C. Patel, M. Yavuz, and S. Nanda, “Femtocells: Industry perspectives,” *IEEE Wireless Commun. Mag.*, vol. 17, no. 5, pp. 6–7, Oct. 2010.
- [4] V. Chandrasekhar, M. Kountouris, and J. G. Andrews, “Coverage in multi-antenna two-tier networks,” *IEEE Trans. Wireless Commun.*, vol. 8, no. 10, pp. 5314–5327, Oct. 2009.
- [5] I. Ashraf, H. Claussen, and L. T. Ho, “Distributed radio coverage optimization in enterprise femtocell networks,” in *Proc. IEEE International Conference on Communications (ICC)*, Cape Town, South Africa, May 23–27, 2010, pp. 1–6.
- [6] O. Simeone, E. Erkip, and S. Shamai (Shitz), “Robust transmission and interference management for femtocells with unreliable network access,” *IEEE J. Sel. Areas Commun.*, vol. 28, no. 9, pp. 1469–1478, Dec. 2010.
- [7] V. Chandrasekhar and J. G. Andrews, “Uplink capacity and interference avoidance for two-tier femtocell networks,” *IEEE Trans. Wireless Commun.*, vol. 8, no. 7, pp. 3498–3509, Jul. 2009.
- [8] H.-S. Jo, C. Mun, J. Moon, and J.-G. Yook, “Interference mitigation using uplink power control for two-tier femtocell networks,” *IEEE Trans. Wireless Commun.*, vol. 8, no. 10, pp. 4906–4910, Oct. 2009.
- [9] Y. J. Sang, H. G. Hwang, and K. S. Kim, “A self-organized femtocell for IEEE 802.16e system,” in *Proc. IEEE Globecom*, Honolulu, HI, Nov.30–Dec.04, 2009, pp. 1–5.
- [10] H.-S. Jo, C. Mun, J. Moon, and J.-G. Yook, “Self-optimized coverage coordination in femtocell networks,” *IEEE Trans. Wireless Commun.*, vol. 9, no. 10, pp. 2977–2982, Oct. 2010.
- [11] P. Xia, V. Chandrasekhar, and J. G. Andrews, “Open vs. closed access femtocells in the uplink,” *IEEE Trans. Wireless Commun.*, vol. 9, no. 12, pp. 3798–3809, Dec. 2010.
- [12] D. Choi, P. Monajemi, S. Kang, and J. Willasenor, “Dealing with loud neighbors: The benefits and tradeoffs of adaptive femtocell access,” in *Proc. IEEE Globecom*, New Orleans, LA, Nov.30–Dec.4, 2008, pp. 1–5.
- [13] “Smartphone review,” TopTen Reviews, 2011. [Online]. Available: <http://cell-phones.toptenreviews.com/smartphones/>
- [14] “Cell phone battery chart,” CNET, 2010. [Online]. Available: <http://reviews.cnet.com/cell-phone-battery-life-charts/?tag=leftNav.0>
- [15] T. S. Rappaport, *Wireless Communications: Principles and Practice*. Upper Saddle River, NJ: Prentice Hall, 2002.
- [16] S. Seidel, T. Rappaport, M. Feuerstein, K. Blackard, and L. Grindstaff, “The impact of surrounding buildings on propagation for wireless in-building personal communications system design,” in *Proc. IEEE VTC*, Denver, CO, May 10–13 1992, pp. 814–815.
- [17] S. Y. Seidel and T. S. Rappaport, “914 MHz path loss prediction models for indoor wireless communications in multifloored buildings,” *IEEE Trans. Antennas Propag.*, vol. 40, no. 2, pp. 207–217, Feb. 1992.
- [18] G. L. Nemhauser and L. A. Wolsey, *Integer and Combinatorial Optimization*, 2nd ed. New York: Wiley-Interscience Publication, 1999.
- [19] H. D. Sherali, W. P. Adams, and P. J. Driscoll, “Exploiting special structures in constructing a hierarchy of relaxations for 0-1 mixed integer problems,” *Operations Research*, vol. 46, no. 3, pp. 396–405, May 1998.
- [20] H. D. Sherali and W. P. Adams, *A Reformulation-Linearization-Technique for Solving Discrete and Continuous Nonconvex Problems*. Boston, MA: Kluwer Academic Publishing, 1999.
- [21] H. D. Sherali and C. H. Tuncbilek, “A global optimization algorithm for polynomial programming problems using a reformulation-linearization technique,” *Journal of Global Optimization*, vol. 2, no. 1, pp. 101–112, 1992.
- [22] H. D. Sherali and H. Wang, “Global optimization of nonconvex factorable programming problems,” *Mathematical Programming*, vol. 89, no. 3, pp. 459–478, 2001.
- [23] H. D. Sherali and J. C. Smith, “Improving discrete model representations via symmetry considerations,” *Management Sciences*, vol. 47, no. 10, pp. 1396–1407, 2001.



Jia Liu (S’03–M’10) received his B.S. and M.S. degrees from South China University of Technology in 1996 and 1999, respectively, both in Electrical Engineering. He also received his B.S. degree in Computer Science from South China University of Technology in 1996. He received his Ph.D. degree in the Bradley Department of Electrical and Computer Engineering at Virginia Tech, Blacksburg, VA in 2010. Since April 2010, he has been working as a Postdoctoral Researcher in the Department of Electrical and Computer Engineering at The Ohio State University. His research focus is in the areas of optimization of communication systems and networks, theoretical foundations of cross-layer optimization on wireless networks, design of algorithms, and information theory. Prior to joining Virginia Tech, Dr. Liu was with Bell Labs, Lucent Technologies in Beijing China from 1999 to 2003.

Dr. Liu is a member of IEEE and SIAM. He is a regular reviewer for major IEEE conferences and journals. He was a recipient of the Bell Labs President Gold Award in 2001, Chinese Government Award for Outstanding Ph.D. Students Abroad in 2008, and IEEE ICC 2008 Best Paper Award. His paper was also the only Runner-up paper of IEEE INFOCOM 2011 Best Paper Award. He served as a TPC member for IEEE INFOCOM 2010 and 2011.



Tianyou Kou received his B.S. in Mathematics from Harbin Institute of Technology in 2003 and M.E. in Electrical Engineering from Chinese Academy of Sciences in 2010. He is now doing a PhD degree in the Department of Electrical and Computer Engineering at The Ohio State University. Prior to joining OSU, he was in the Center for Earth Observation and Digital Earth in Beijing China from 2009 to 2010. His research focus is in the areas of nano-communication, Internet of Things, algorithms and optimization.



Qian Chen received her B.E. degree in Architecture from Southwest Jiaotong University in China in 1996 and an M.E. degree in Civil Engineering from National University of Singapore in 2003. She received a second M.S. degree in Architecture in 2004 and her Ph.D. degree in Environmental Design and Planning/Building Construction in 2007, both from Virginia Tech, Blacksburg, VA. Before coming to U.S., she had six years of construction industry work experiences. Since 2007, Dr. Chen has been an Assistant Professor of Construction Systems Management at The Ohio State University. Her research focuses on Interface Management in Integrated Project Delivery, Building Information Modeling, IT Applications in Construction Management, Lean Construction, and High Performance Green Buildings. She is a LEED Accredited Professional, an associate member of American Society of Civil Engineers (ASCE), and a member of American Society for Engineering Education.



Hanif D. Sherali is a University Distinguished Professor and the W. Thomas Rice Chaired Professor of Engineering in the Industrial and Systems Engineering Department at Virginia Polytechnic Institute and State University. His areas of research interest are in analyzing problems and designing algorithms for specially structured linear, nonlinear, and integer programs arising in various applications, global optimization methods for non-convex programming problems, location and transportation theory and applications, and economic and energy mathematical modeling and analysis. He has published over 290 refereed articles in various Operations Research journals, has (co-) authored eight books in this area, and serves on the editorial board of eight journals. He is a Fellow of INFORMS and IIE, and an elected member of the National Academy of Engineering.